Li-ion Battery Cell Aging Observation based on Impedance Spectroscopy

Miroslav Novák[1]

[1] Technical University of Liberec, Studentska 2, 461 17 Liberec, The Czech Republic
miroslav.novak@tul.cz

Abstract. The lithium battery's state of health is an essential index for characterization. It is crucial, for example, to estimate the range of an electric car. Electrochemical impedance spectroscopy is a relatively simple diagnostic tool for insight into the cell's internal processes. Impedance spectra can be used to estimate temperature, state of charge, and also the state of health, which is presented in this paper. High power 18650 cells were cycled down to 80 % of their original capacity. The impedance spectra were measured at regular intervals during cycling. Impedances were measured separately for each frequency in the range 5 mHz to 5 kHz. A galvanostatic method was used to excite the cells. The parameters of the cell equivalent circuit were identified from the measured set of the impedance spectra. The results show an evident dependence on the ohmic resistance of the current collectors and electrodes, also the dependence of the resistance and capacity of the electrochemical double layer on the number of discharge cycles.

Keywords: Electrochemical impedance spectroscopy, Li-ion battery, Capacity fade.

1 Introduction

In the last decade, Li-ion batteries have taken a leading place in mobile handheld applications, hand tools, embedded systems, electromobility, and as stationary energy storage. The reason for the success of Li-ion batteries is primarily their excellent energy density, along with a high number of charge cycles and high charge/discharge currents. The weakness of these batteries is a thermal runaway, potentially ending in an explosion or fire. Reducing the risk of thermal runaway is achieved by a combination of additives in the electrolyte, a temperature-sealable separator, an overpressure valve, an overcurrent limiter, and electronic supervision in the form of a battery management system (BMS).

Massive sales volumes bring the need and, at the same time, finances to optimize the parameters mentioned above. Individual parameters influence each other to a different degree and direction. The design of the battery is therefore a complex technical-economic compromise.

The material, the construction of the electrodes, the separator, and the composition of the electrolyte has an influence of battery performance. As a standard, measuring the

M. Petr et al. (eds.), *62nd International Conference of Machine Design Departments (ICMD 2022)*,
Atlantis Highlights in Engineering 28,
https://doi.org/10.2991/978-94-6463-423-5_41

discharge characteristic and the drop in capacity with the lifecycle is used. This decrease in capacity is called the state of health (SoH). For detailed monitoring of the cell damage after the number of cycles, microscopic and material analysis is performed after disassembly. This cell destruction makes it impossible to continue the test with further load cycles. The experiment must be designed with a large number of samples, and it is therefore costly.

Electrochemical impedance spectroscopy (EIS) is a technique for measuring the frequency dependence of a cell's impedance (internal resistance), making it possible to distinguish phenomena at current collectors, at the electrode-electrolyte interface, and the migration of lithium ions in the electrodes [1]. Thus, EIS enables insight into the cell properties without needing to open them. Therefore, EIS is a non-destructive and relatively fast method, which is why it is becoming more and more popular.

The first compilation is the interpretation of the EIS results. Impedance is influenced not only by the condition of the electrodes (SoH) [2, 3], i.e., their degradation. Other essential factors are the state of charge (SoC) and cell temperature [4, 5]. If we are concerned with a narrow spectrum band, EIS can be used to measure the internal temperature of a cell [6, 7, 8].

EIS is also used in other areas of the industry, including coatings, anodized films, corrosion inhibitors, and fuel cells. EIS is not entirely standardized, which is the second complication. Either voltage excitation (potentiostatic method) or current excitation (galvanostatic method) is used. Different authors use different magnitudes of currents and voltages. In the articles, the exact parameters of measurement and data processing are often not given. However, they have a significant impact on the results [9]. Therefore, the results of partial research are difficult to compare.

The aim of this study is to present the results of EIS changes during the life cycle of Li-ion cells. Measured data are interpreted using numerical identification of equivalent circuit parameters. The effort is to provide as accurate a description of the measurement method.

2 Materials and methods

This section describes selected cells and the cyclic loading methodology, a description of the measuring apparatus, the EIS measurement procedure, and the equivalent circuit used for the mathematical description of the cell.

2.1 Li-ion cell samples

A standard cylindrical cell with high discharge current SAMSUNG INR18650-25R was selected for the tests. These are commonly used cells for laptops, portable power, instrumentation, digital cameras, electronic cigarettes, and other applications. The cell chemistry is LiNiCoAlO2 (NCA). The main features are given in table 1. These cells were chosen for high current load and, thus, relatively short charge-discharge cycles. A set of 6 cells from the same production batch was used for the tests.

Table 1. Parameters of cells used in the test.

Quantity	Value	Quantity	Value
Capacity	2500 mAh	Standard charging current	1.25 A (0.5C)
Nominal voltage	3.6 V	CV current	0.125 A (0.05C)
Maximal voltage	4.2 V	Standard disch. current	0.5 A (0.2C)
Minimal voltage	2.5 V	Maximal charging current	4 A (1.6 C)
Operating charging temperature	0–50 °C	Maximal disch. current	20 A (8C)
Operating disch. temperature	-20–75 °C	Cycle life (to 80 % capacity)	250 (100 % DoD, 25 °C)

2.2 Aging cycles

The aging test consisted of cycling cells to a 100 % capacity using the Chroma 17011 Battery Cell Charge/Discharge Test System. All six cells were cycled simultaneously, each on its tester channel. The charging current of 1.6C in CCCV charging mode was used in the test. Then it was followed by a pause of 2 minutes and discharge with a discharge current of 1.6C, followed by a delay of 2 minutes. The maximum charge and high discharge current were chosen to speed up the test.

EIS was measured after the first cycle and then every other 62 cycles. The last cycle before the EIS measurement was completed at a state of charge (SoC) of 60% of the nominal capacity. 60% SoC was chosen with regard to avoiding events of solid-electrolyte interface (SEI) impedance changes that occur at about 45% SoC and also avoiding the extreme areas close to the cell complete discharge and full charge, where the impedance spectrum is significantly different.

A measurement sequence of discharge cycles followed by EIS measurement was performed until the capacity drops to 80%, which was considered as battery end of life. The Chroma 17011 tester recorded the actual cell capacity from every discharge in each aging cycle. The cells were cycled at the temperature given by the environment in the laboratory. Minor fluctuations of ±2 °C also caused slight changes in the measured cell capacity.

The results are shown in Fig. 4. The cycles in which the EIS measurement was performed are also marked here.

2.3 EIS

The setup for EIS measurement uses galvanostatic methods. The apparatus enables the simultaneous measurement of two cells to speed up the measurement. Excitation is provided by a pair of voltage-controlled current sources OPA549. The cDAQ NI 9263 DAC module generates the control signal for the sources. The NI 9239 ADC module senses the cell voltage and NI 9227 senses current with a sampling frequency of 50 kSPS and synchronous channel sampling. The DAC and the ADC modules have a coupled trigger signal to start the measurement. The measured Li-ion cells are

connected via four-wire holders to eliminate the impedance of the connecting wires and contact points.

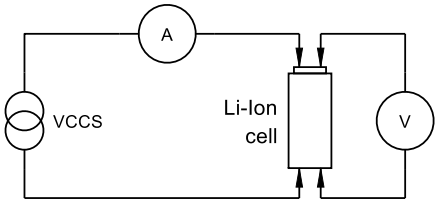

Fig. 1. Scheme of the galvanostatic method

The measurement was performed at 36 discrete points evenly divided logarithmically over the range of 5 mHz to 5 kHz. The measurement proceeds from higher to lower frequencies. Individual frequencies are rounded so that they are integer divisible by the sampling frequency of the measuring system. The length of the generated sinusoidal signal is at least 1 second, and the signal must contain at least three full signal periods. Shortened periods are eliminated, ensuring that no cell's parasitic charging/discharging occurs during the test. A delay of 3 seconds is inserted between the measurements of individual points to stabilize changes in the electrochemical potential. For this reason, the initial minimum of 0.2 seconds and at least the first period are also excluded from the impedance calculation. The signal is trimmed so that the whole number of periods is in the processed area.

Although the excitation is galvanostatic, it means the independent harmonic current is generated; the current amplitude is controlled so that the amplitude of the voltage drop on the cell is close to 10 mV. The regulation is to maintain the electrochemical process in the linear region. Therefore, the limit voltage must not be exceeded. Details are documented in [10].

The calculation of magnitudes $|\mathbf{U}(f)|$ resp. $|\mathbf{I}(f)|$ and phases $\varphi_{\mathrm{U}}(f)$ and $\varphi_{\mathrm{I}}(f)$ is performed by fast Fourier transformation. The frequency for evaluation f was the excitation frequency, which corresponds to the fundamental harmonic h_1 of the resulting spectrum. The complex impedance is calculated from values at exciting frequency line

$$\mathbf{Z}(f) = \frac{\mathbf{U}(f)}{\mathbf{I}(f)} = \frac{|U(f=h_1)|}{|I(f=h_1)|} e^{j(\varphi_{\mathrm{I}} - \varphi_{\mathrm{U}})}. \tag{1}$$

2.4 Equivalent circuit model

The curves of the impedance spectra reflect different processes in the battery in their various parts [11, 12, 1, 13, 14], see Fig. 2. The high-frequency region (R_e) reflects the ohmic resistance of the electrodes and the current collectors of the cell and inductance (L_e) mainly caused by the porous nature of electrodes. At high frequencies (CPE_h), the impedance reflects the migration of lithium ions through the SEI film. In the middle frequency range (CPE_m), the capacity of the electric double layer on the surface of the electrodes manifests itself. The diffusion of ions into the material of the electrodes is

displayed at low frequencies (CPE_l / W_d). However, the individual bands more or less overlap. Additionally, the parameters change with temperature, SoC, and SoH. For example, the CPE_h and CPE_m regions sometimes merge entirely into one arc. This complexity of internal battery phenomena makes interpretation of the results difficult.

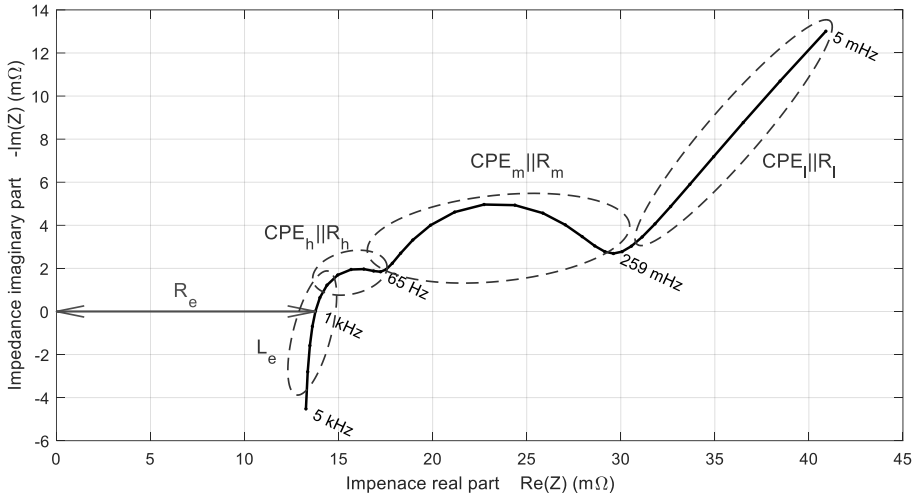

Fig. 2. EIS curve in the complex plane with the marked areas

Therefore, the Equivalent Circuit (EC) description is used to ease interpretation. The EC model consists of series-parallel *RLC* circuit elements representing partial electrochemical processes. Special elements such as constant phase element (CPE), Warburg impedance, linear diffusion element, or Gerischer impedance are also often included; see Tab. 2. The construction of EC models is not standardized, and we can find many variants in scientific articles.

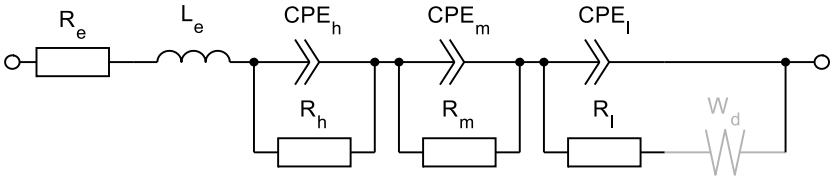

Fig. 3. Equivalent circuit for cell impedance used in this article

Table 2. Overview of elements used in EC electrochemical cells.

Element	Marking	Impedance (Ω)
Resistor	R	$Z_R = R$
Inductor	L	$Z_L = j\omega L$
Capacitor	C	$Z_C = \frac{1}{j\omega C}$

Constant phase element	CPE, Q	$Z_{CPE} = \frac{1}{Q(j\omega)^{\alpha}}$
Warburg impedance for infinite diffusion	W	$Z_W = \frac{\sigma\sqrt{2}}{\sqrt{j\omega}}$
Warburg impedance for convective diffusion	W_d	$Z_{Wd} = R_d \frac{\tanh\left(\sqrt{\tau_d j\omega}\right)}{\sqrt{\tau_d j\omega}}$
Linear diffusion element	M	$Z_M = R_d \frac{\coth\left(\sqrt{\tau_d j\omega}\right)}{\sqrt{\tau_d j\omega}}$
Gerischer impedance	G	$Z_G = \frac{R_d}{\sqrt{1+\tau_d j\omega}}$

Many authors use multiple combinations of elements. Although the elements logically describe the physical essence, they are often duplicated from a mathematical point of view. The EC model is then over-determined, and when searching for parameters, some elements can compensate for the influence of others [15]. The actual search is complicated and time-consuming, and the results may not be correct. When using simpler models with fewer elements, the physical phenomena inside the cell are not sufficiently defined, and the model deviates more from measurements.

3 Results and discussion

The results of the aging test are shown in Fig. 4. The cell capacity determined by the Chroma tester from the discharge part of the cycle is plotted on the vertical axis. SoH is written parallelly in parentheses in gray font. The manufacturer's guaranteed number of cycles of 250 was exceeded more than twice.

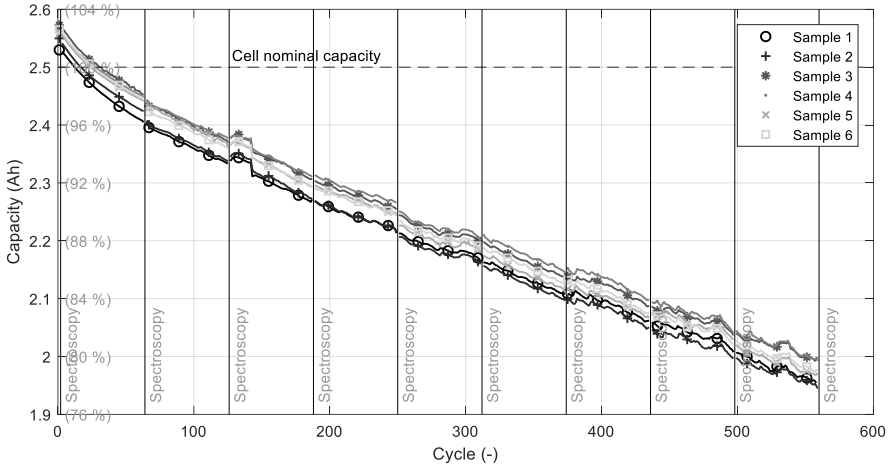

Fig. 4. Decrease in the capacity of the tested cells depending on the number of discharge cycles. The vertical lines represent the cycles in which the impedance spectroscopy was measured.

Individual cells did not have the same initial capacity. Cell three showed the highest capacity of 102.74 % nominal value, while cell one had 101.08 %. The trend of the capacity drop was very similar for all cells. In the first approx. 150 cycles, the decline was steeper. The further decline was approximately linear. At the end of aging, after 559 cycles, the capacity dropped to 78.8% on average. Cell no. 2 finished worst with 77.8 %. It can be stated that the measured lifetime was twice as long as declared.

Fluctuations in temperature during the test caused the slight ripple of the waveforms. Small step changes in capacity before and after the ISE measurement are probably caused by the time delay that was needed to perform the ISE on the second apparatus, where the cells were measured sequentially. In some cases lasted up to 3 days.

The progression of the impedance spectra depending on the completed cycles is shown in Fig. 5. For clarity, curves are offered only for cell no. 3, and only every other curve is shown. The parameters of the EC model identified from these curves are then shown in Fig. 6.

The impedance of all parts of the curves gradually increases with aging. In the area of high frequencies (left-hand side), the shift of the curves is visible. This is the increase in the current collector resistance caused by its gradual corrosion and cracks in the active electrode layer. The R_e subgraph of Fig. 6 well documents this growth. Here, it is worth paying attention to the acceleration of degradation in cells no. 1 and 2 after undergoing 300 and 450 cycles, respectively. The R_e correlates with SoH drop.

The inductive drop in the imaginary component of the impedance -Im(**Z**) in the high-frequency region is hardly visible. The series inductance L_e increases only very slightly, according to the identified parameters of the model by only 10%.

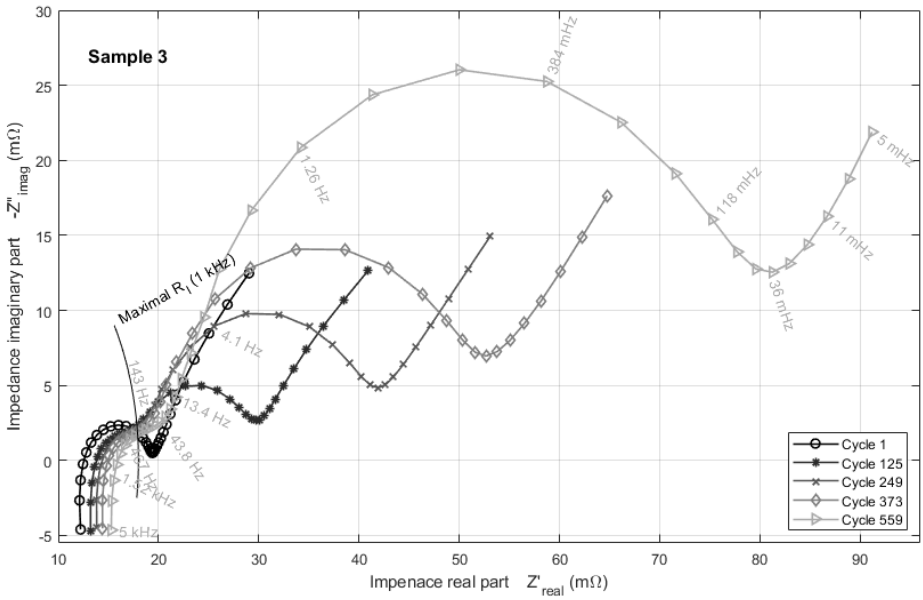

Fig. 5. Change of the impedance spectrum depending on the number of discharge cycles of the cell.

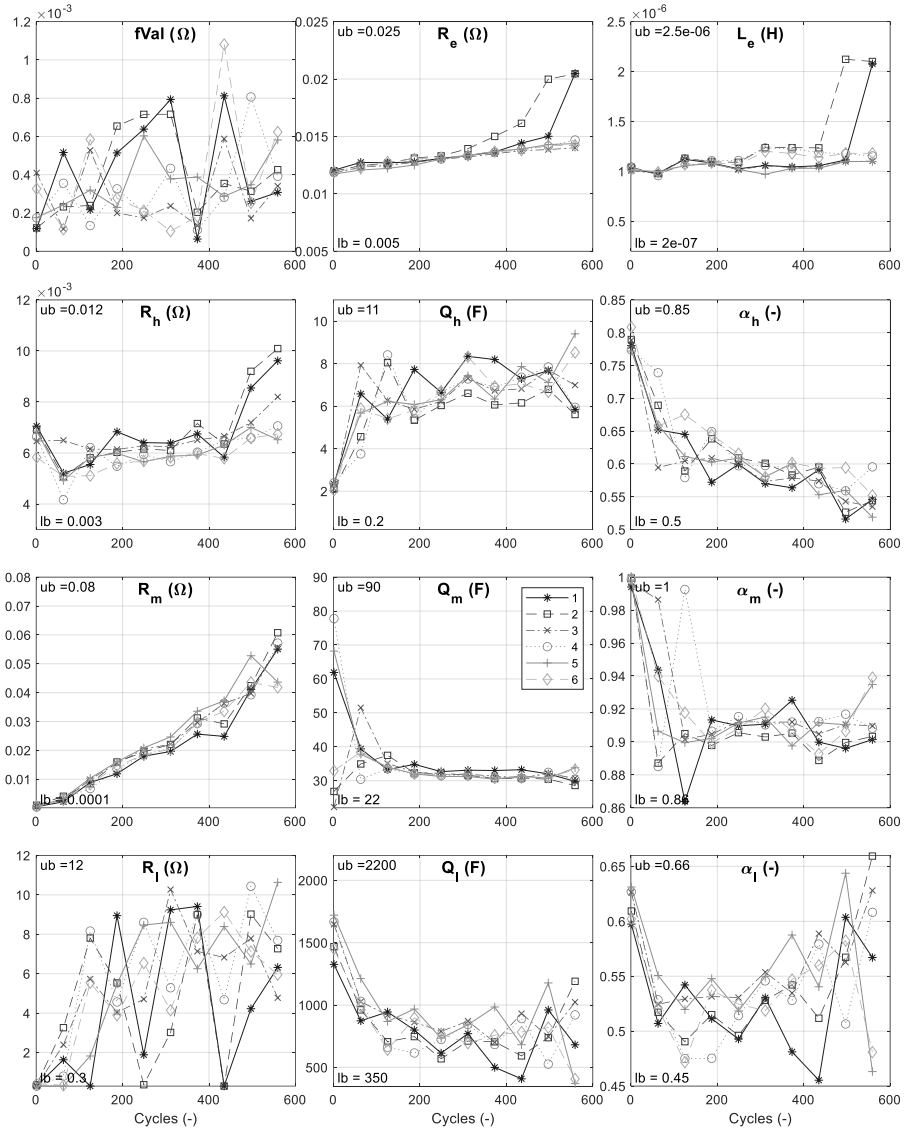

Fig. 6. Estimated model parameters depending on the number of discharge cycles.

Parameters of the equivalent circuit, according to Fig. 3 were identified for all cells from the measured impedance spectra. The results are shown in Fig. 6 and 7, respectively.

A simplified EC model was chosen. The main difference compared to the used models is the term CPE_l in the area of very low frequencies describing the diffusion of Lithium ions into the material of the electrodes. Here, a linear diffusion CPE element is typically used in parallel with a resistor and a Watburg impedance. However, the performed measurements end at a frequency of 5 mHz. The data contains only about

5-7 points in the area of low frequencies. The information contained is not sufficient for a good identification of the complex model, so the Warburg impedance has been omitted. The fit of such a simplified model is sufficient for the given inputs.

The model parameters were searched using nonlinear optimization with a limited range of input parameter values. The correct setting of the limits for the searched parameters is key to achieving the correct outputs. As mentioned above, jump swaps between CPE||R groups occur in case of inappropriate settings. From a physical point of view, we expect Q values in each group to be in a different range; their course with the change of SoH is expected to be continuous. An example of not entirely correct identification can be found, for instance, in [15]. The setting of the lower limit *lb* during identification is indicated for each parameter in the lower left corner of the corresponding subgraph. Similarly, the upper limit *ub* is shown in the upper left corner.

The criterion function f'_{Val} used for optimization is also worth mentioning. The optimization was performed as the sum of the deviations of the real and imaginary parts of the measured impedance $\mathbf{Z}_{\mathrm{m}}$ and equivalent circuit approximated impedance $\mathbf{Z}_{\mathrm{a}}$. A commonly used quadratic criterion [16]

$$f'_{Val} = \sum_k \left[\left(\mathrm{Re}\left(\mathbf{Z}_m(k)\right) - \mathrm{Re}\left(\mathbf{Z}_a(k)\right) \right)^2 + \left(\mathrm{Im}\left(\mathbf{Z}_m(k)\right) - \mathrm{Im}\left(\mathbf{Z}_a(k)\right) \right)^2 \right] \quad (2)$$

does not lead to good and stable results in the entire range of SoH. The minimization of the sum of deviations proved to be the most effective

$$f'_{Val} = \sum_k \left[\left| \mathrm{Re}\left(\mathbf{Z}_m(k)\right) - \mathrm{Re}\left(\mathbf{Z}_a(k)\right) \right| + \left| \mathrm{Im}\left(\mathbf{Z}_m(k)\right) - \mathrm{Im}\left(\mathbf{Z}_a(k)\right) \right| \right]. \quad (3)$$

The first subgraph in Fig. 6 shows the average deviation per point for a set of found parameters

$$f_{Val} = f'_{Val}/(2N), \quad (4)$$

where N is the number of measured points, the deviation will come out in Ohms (Ω).

Identifying the data of new and less cycled cells in the case of parameter changes on the SoH, where the first and second semicircles overlap, is critical. This is evident in the increased variances of the parameters Q_{h}, Q_{m}, R_{h} at the first few points from the left. As the cells degrade, the semicircle separates, and the identification is stable.

The instability of the results for Q_{l}, R_{l}, α_{l} is due to the small number of points in the input data, as already mentioned. The high variances are visible in the boxplots in Fig. 7.

The reliable parameters for estimating SoH are the resistance R_{e} and the CPE parameters for semicircles at medium frequencies R_{m} and Q_{m}, which cause changes in the electric double layer. This is evident from the results in Fig. 7. The mentioned parameters are also not very sensitive to the precise setting of the limits when identifying the equivalent circuit parameters.

The dependence of R_{e} on SoH, respective to the number of cycles c, is linear as in [17]. The equation can approximate it

$$R_e = 4.5^{-3}c + 12\ (m\Omega). \tag{5}$$

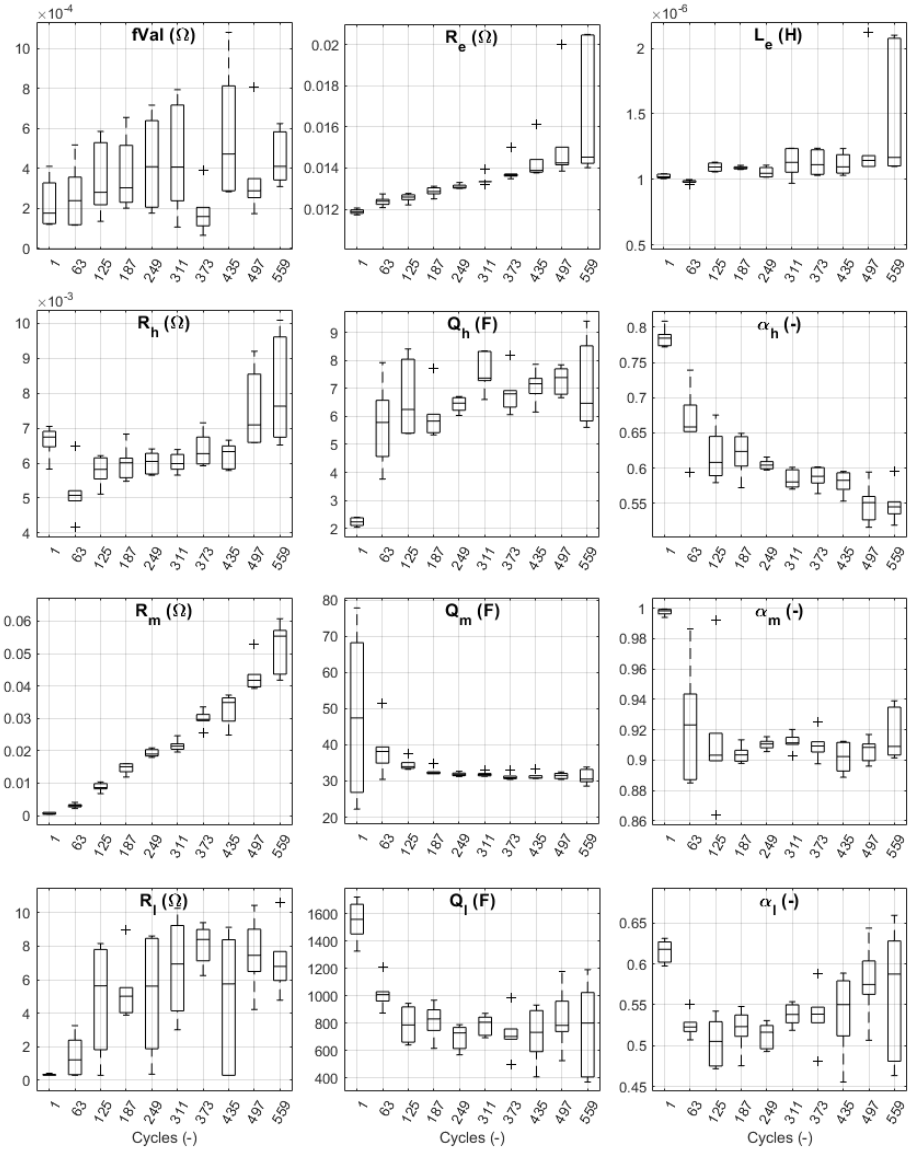

Fig. 7. Boxplots of estimated model parameters depending on the number of discharge cycles.

The input data for the approximation $R_e(c)$ were medians from measurements on six cells to exclude the influence of cell 1 and 2 degradation changes.

The approximation of resistance R_m is also approximately linear, given by

$$R_m = 92^{-3}c - 2.8\ (m\Omega). \tag{6}$$

The capacitance of the constant phase at medium frequencies was approximated by an exponential function

$$Q_m = 0.9865^{(c-207)} + 31.0\ (F). \tag{7}$$

4 Conclusions

EIS measurement is a convenient non-destructive test of battery cells. For electrochemical cells, the galvanostatic method has the advantage that it does not need DC excitation separation. With sufficient voltage and current measurement accuracy and correct signal processing, it gives stable and accurate results of cell impedance spectra.

The waveforms obtained can be used to identify the parameters of the equivalent circuit. The equivalent circuits used do not guarantee the non-interchangeability of individual sections. Therefore, it is necessary to limit the range of parameters of the circuit elements during identification. The changes in circuit parameters with SoH are significant. Finding robust limits for circuit element values is not easy. For future investigation, it would be appropriate to develop sliding limit methods.

The parameters R_e, Q_m, R_m, correlate well with SoH and can therefore be recommended for its estimation under measurement conditions at the same SoC and temperature. The model used is sensitive to the bounds setting when searching for the size of the parameters.

Acknowledgements

The result was obtained through the financial support of the Ministry of Education, Youth and Sports of the Czech Republic and the European Union (European Structural and Investment Funds – Operational Programme Research, Development and Education) in the frames of the project “Modular platform for autonomous chassis of specialized electric vehicles for freight and equipment transportation”, Reg. No. CZ.02.1.01/0.0/0.0/16_025/0007293.

References

1. Dai, H., Jiang, B., Wei, X.: Impedance Characterization and Modeling of Lithium-Ion Batteries Considering the Internal Temperature Gradient. Energies 11, 220. (2018) https://doi.org/10.3390/en11010220.
2. Liebhart, B., Diehl, S., Endisch, C.: Sensitivity Analysis of Battery Cell Aging Estimators based on Impedance Spectroscopy regarding Temperature Compensation. In: 2020 IEEE Conf. on Control Technology and Applications (CCTA), pp. 801–806. (2020) https://doi.org/10.1109/CCTA41146.2020.9206395.
3. Tröltzsch, U., Kanoun, O., Tränkler, H.-R.: Characterizing aging effects of lithium ion batteries by impedance spectroscopy. Electrochimica Acta 51, 1664–1672. (2006) https://doi.org/10.1016/j.electacta.2005.02.148.

4. Mirzaei, H., Li, Z., Parvini, Y.: Validation and Sensitivity Analysis of a Fractional Order Model of a Lithium Ion Battery via Impedance Spectra and Temporal Duty Cycles. In: 2020 American Control Conference (ACC), pp. 359–364. (2020) https://doi.org/10.23919/ACC45564.2020.9147573.
5. Skoog, S., David, S.: Parameterization of linear equivalent circuit models over wide temperature and SOC spans for automotive lithium-ion cells using electrochemical impedance spectroscopy. Journal of Energy Storage 14, 39–48. (2017) https://doi.org/10.1016/j.est.2017.08.004.
6. Beelen, H.P.G.J., Raijmakers, L.H.J., Donkers, M.C.F., Notten, P.H.L., Bergveld, H.J.: An Improved Impedance-Based Temperature Estimation Method for Li-ion Batteries. In 4th IFAC Workshop on Engine and Powertrain Control, Simulation and Modeling E-COSM, pp. 383–388. (2015) https://doi.org/10.1016/j.ifacol.2015.10.055.
7. Hussein, A.A., Fardoun, A.A.: An Adaptive Sensorless Measurement Technique for Internal Temperature of Li-Ion Batteries Using Impedance Phase Spectroscopy. IEEE Trans. on Industry Applic. 56, 3043–3051. (2020) https://doi.org/10.1109/TIA.2020.2979783.
8. Raijmakers, L.H.J., Danilov, D.L., Lammeren, J.P.M. van, Lammers, T.J.G., Bergveld, H.J., Notten, P.H.L.: Non-Zero Intercept Frequency: An Accurate Method to Determine the Integral Temperature of Li-Ion Batteries. IEEE Trans. on Indust. Electronics 63, 3168–3178. (2016) https://doi.org/10.1109/TIE.2016.2516961.
9. Hang, T., Mukoyama, D., Nara, H., Takami, N., Momma, T., Osaka, T.: Electrochemical impedance spectroscopy analysis for lithium-ion battery using Li4Ti5O12 anode. Journal of Power Sources 222, 442–447. (2013) https://doi.org/10.1016/j.jpowsour.2012.09.010.
10. Haußmann, P., Melbert, J.: Optimized mixed-domain signal synthesis for broadband impedance spectroscopy measurements on lithium ion cells for automotive applications. J. Sens. Sens. Syst. 6, 65–76. (2017) https://doi.org/10.5194/jsss-6-65-2017.
11. Andre, D., Meiler, M., Steiner, K., Wimmer, Ch., Soczka-Guth, T., Sauer, D.U.: Characterization of high-power lithium-ion batteries by electrochemical impedance spectroscopy. I. Experimental investigation. Journal of Power Sources 196, 5334–5341. (2011) https://doi.org/10.1016/j.jpowsour.2010.12.102.
12. Lyu, C., Wei, G., Wen, Z., Zhang, H., Wu, Q., Jing, H.: Research on the Performance Evaluation of Lithiumion Battery Cascade Utilization Based on Impedance Spectrum. In 15th IEEE Conf. on Indust. Electronics and Applications (ICIEA), pp. 1714–1719. (2020) https://doi.org/10.1109/ICIEA48937.2020.9248404.
13. Osaka, T., Nara, H., Mukoyama, D., Yokoshima, T.: New Analysis of Electrochemical Impedance Spectroscopy for Lithium-ion Batteries. J. Electrochem. Sci. Technol 4, 157–162. (2013) https://doi.org/10.33961/JECST.2013.4.4.157.
14. Krčmář, L., Rydlo, P., Richter, A., Eichler, J., Jandura, P.: State of Health and Aging Estimation Using Kalman Filter in Combination with ARX Model for Prediction of Lifetime Period of Li-Ion. In *Intern. Conf. on Electrical Drives & Power Electronics (EDPE),* pp. 234-237, (2021) https://doi.org/10.1109/EDPE53134.2021.9604098.
15. Xia, Z., Qahouq, J.A.A.: Evaluation of Parameter Variations of Equivalent Circuit Model of Lithium-ion Battery under Different SOH Conditions. In: 2020 IEEE Energy Conversion Congress and Exposition (ECCE), pp. 1519–1523. (2020) https://doi.org/10.1109/ECCE44975.2020.9236339.
16. Wang, X., Dai, H., Jiang, B.: Research on Impedance and Nonlinear Characteristics of Lithium-Ion Batteries. In: IEEE Vehicle Power and Propulsion Conf. (VPPC). pp. 1–6. (2018) https://doi.org/10.1109/VPPC.2018.8604963.
17. Lyu, C., Zhang, T., Luo, W., Wei, G., Ma, B., Wang, L.,: SOH Estimation of Lithium-ion Batteries Based on Fast Time Domain Impedance Spectroscopy. In: 14th IEEE Conf. on

Industrial Electronics and Applications (ICIEA). pp. 2142–2147. (2019) https://doi.org/10.1109/ICIEA.2019.8834119.